AIAA 80-0255R

Aerodynamic and Inlet Flow Characteristics of Several Hypersonic Airbreathing Missile Concepts

James L. Dillon,* Don C. Marcum Jr.,* Patrick J. Johnston,* and James L. Hunt*
NASA Langley Research Center, Hampton, Va.

Four conceptual hypersonic missile configurations were examined experimentally and theoretically. Two of the concepts employed twin module bottom-mounted engines and two were designed for upper-surface inlets or engines with the intent of reducing the vehicle observables. The tests were conducted at Mach 6 and Reynolds numbers of 6 to 7.5×10^6/ft. Flowfield surveys in the vicinity of the engine inlet were made on all configurations and force and moment tests were conducted on three of the vehicles. Stability and control characteristics of the bottom-mounted engine configurations which incorporated low, slender wings were dominated by strong vortices that promoted severe pitchup tendencies. The shock layer and flow quality in the vicinity of the bottom-mounted engine inlets were dependent on nose shape. The spatula-like upper-surface engine concept demonstrated good performance and had uniform flow entering the engine inlet, while the upper-surface inlet concept with a highly swept forebody incurred large gradients due to interactions with leading-edge shocks.

Nomenclature

b	= wing span
B.L.	= boundary layer
C_D	= drag coefficient, drag/$q_\infty S$
C_L	= lift coefficient, lift/$q_\infty S$
C_l	= rolling moment coefficient, rolling moment/$q_\infty Sb$
C_{l_β}	= rate of change of C_l with sideslip angle, per deg
C_m	= pitching moment coefficient, pitching moment/$q_\infty Sl$
C_{m_α}	= rate of change of C_m with angle of attack, per deg
C_{m_δ}	= rate of change of C_m with control deflection, per deg
C_n	= yawing moment coefficient, yawing moment/$q_\infty Sb$
C_{n_β}	= rate of change of C_n with sideslip angle, per deg
C_p	= pressure coefficient, $(p-p_\infty)/q_\infty$
l	= model length
L/D	= lift-drag ratio
M	= Mach number
p	= static pressure
P	= total pressure
q	= dynamic pressure
S	= reference area
x,y,z	= distance along X, Y, and Z axis, respectively
X,Y,Z	= longitudinal, lateral, and vertical axis, respectively
α	= angle of attack
β	= angle of sideslip
δ_T	= tail deflection

Subscripts

max	= maximum
0	= conditions at zero lift
p	= probe
T	= total conditions
∞	= freestream

Introduction

RECENT conceptual studies[1-3] indicate that hypersonic airbreathing missiles may provide attractive overall performance. The classes of configurations reflected in these studies contrast to aircraft as being more slender with lower aspect ratio aerodynamic surfaces and large volume bodies in relation to the size of lifting surfaces. Consequently, they present different aerodynamic problems which must be explored with equal thoroughness. Examples which quickly come to mind are the potential for component shielding or adverse interference due to the close proximity of control surfaces to the wings. Hypersonic-airbreathing missiles may have additional problems relating to the quality and size of the flowfield available to the engine inlet, especially in high g maneuvering conditions.

The existing data base for shapes that are envisioned as representative for this class of hypersonic vehicles is sparse

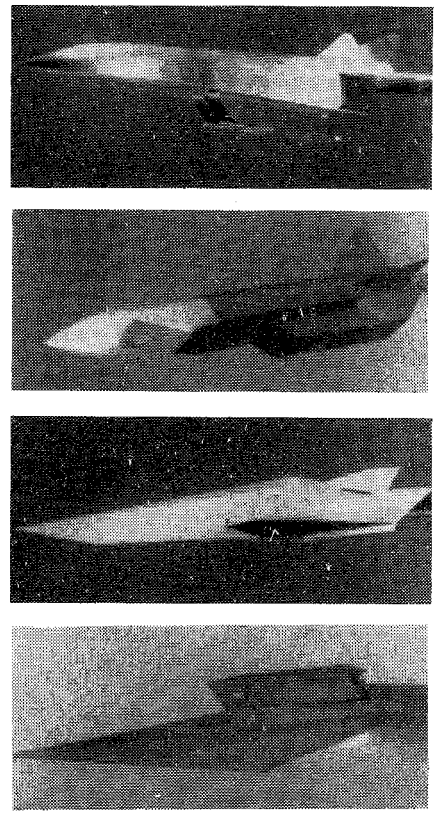

Fig. 1 Photograph of hypersonic airbreathing missile study concepts.

Received Jan. 9, 1980; presented as Paper 80-0255 at the AIAA 18th Aerospace Sciences Meeting, Pasadena, Calif., Jan. 14-16, 1980; revision received Sept. 22, 1980. This paper is declared a work of the U.S. Government and therefore is in the public domain.

*Aerospace Engineer. Hypersonic Aerodynamics Branch, High-Speed Aerodynamics Division. Member AIAA.

and the usage of current prediction techniques that have been successfully employed on airplane-like configurations for missile shapes is open to question. To help alleviate this scarcity of data and to provide an initial assessment of current theoretical techniques, models of four hypersonic air-breathing missile configuration concepts have been tested.

The first two configurations (A and B, Fig. 1) were formulated about modular dual-mode scramjets nested to the lower fuselage where the forebody provides both lift and engine air-flow compression and the aft end acts as a high-expansion ratio nozzle. Both of these concepts would require a rocket booster to achieve a staging Mach number of 4 or greater. The principal differences in these configurations are in the blending of the nose/fuselage/wing region, and, to a lesser extent, in engine sizing which is dependent on mission objectives. The second two configurations (C and D, Fig. 1) would accommodate top-mounted inlets and were derived from stealth considerations; however, they differ considerably in engine integration philosophy and forebody design.

All experimental data were obtained at Mach 6 at Reynolds numbers from 6 to 7.5×10^6/ft. Force and moment data including component effects were obtained on three of the models. In addition, flowfield surveys were conducted near the engine-inlet face of each model since forebody boundary layer and inviscid shock-layer characteristics are configuration oriented and impact the location and performance of the airbreathing engine.

This paper reports on the initial results of the experimental data and comparisons with theory.

Models, Apparatus, and Tests

The experimental data presented herein were measured on metal models mounted in the Langley Research Center Mach 6, 20-in. tunnel. The models were fabricated with interchangeable parts and movable control surfaces in order to investigate overall component effects. The force and flowfield tests were conducted at Reynolds number per foot ranging from 6 to 7.5×10^6.

For the force tests, the models were mounted on internal, six-component strain-gage balances which were attached to the tunnel sting-support system. A representative two-module flow-through scramjet package was included as part of the component buildup. The nacelle package used in this test simulated the internal geometric contraction of a representative engine by use of a single strut. The overall engine effect on performance requires tests with a thrusting engine using a simulant gas which is beyond the scope of this investigation. However, the effects of the nonthrusting engine are representative of a power-off segment of the flight profile or an end game situation. All test results were adjusted to correspond to free-stream static pressure acting over the model base.

The flowfield investigations were conducted with a pitot tube which traversed from the model wall through the fuselage bow shock. The stainless steel-probe tip was approximately elliptical with the major axis 0.035 in., the minor axis 0.024 in., and the wall thickness 0.006 in. Static-pressure orifices were located on the model in the vicinity of the survey station. Prior to a test, the model was heated to near adiabatic conditions as determined by a thermocouple mounted inside the model.

Theoretical Methods

The Hypersonic Arbitrary-Body Aerodynamics Program (Ref. 4) was used to predict the forces and moments on all configurations. Following past experience, tangent-cone theory was used to predict pressures on windward-body surfaces and the tangent-wedge option was used on windward-planar lifting surfaces. A Prandtl-Meyer expansion from the freestream was used on all leeward surfaces with the pressure coefficient limited to $C_p = -1/M_\infty^2$. Skin friction was predicted using the Spalding-Chi method assuming the boundary layer to be fully turbulent.

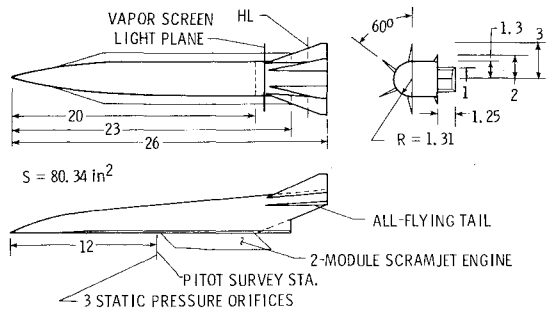

Fig. 2 Sketch of concept A, dimensions in inches.

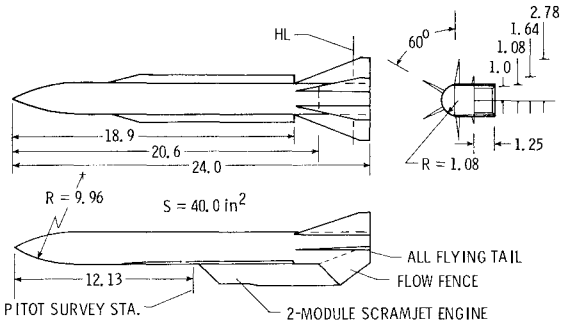

Fig. 3 Sketch of concept B, dimensions in inches.

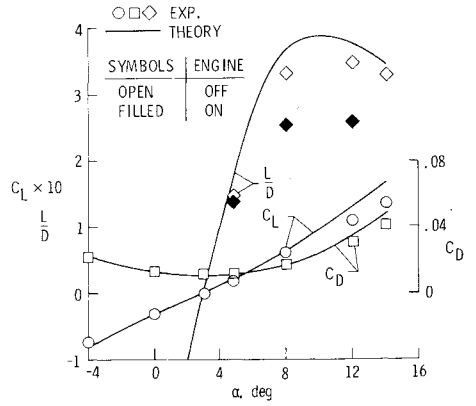

Fig. 4 Aerodynamic performance characteristics of concept A.

Concepts, Results, and Discussion

Bottom Surface Engine Concepts

Concepts A and B

A sketch of concept A is shown in Fig. 2. This shape resulted from an effort to configure a vehicle envisioned for long range cruise missions at hypersonic speeds. The forebody-lower surface and low-wing placement was designed to provide a uniform, precompressed flowfield to the inlet of the integrated modular engine at cruise angles of attack, while the lower afterbody provides a high-expansion-ratio, low-drag nozzle. The narrow wings provide short leading-edge lengths, overall structural efficiency, low heat loads, and compactness. Stability and control is provided by all-flying horizontal tails and stationary side fins. The tails had approximately 53% greater semispan than the wing.

A sketch of concept B is shown in Fig. 3. This vehicle was configured for a tactical-like mission with certain features such as the flat-bottom high-expansion nozzle, "D" shaped

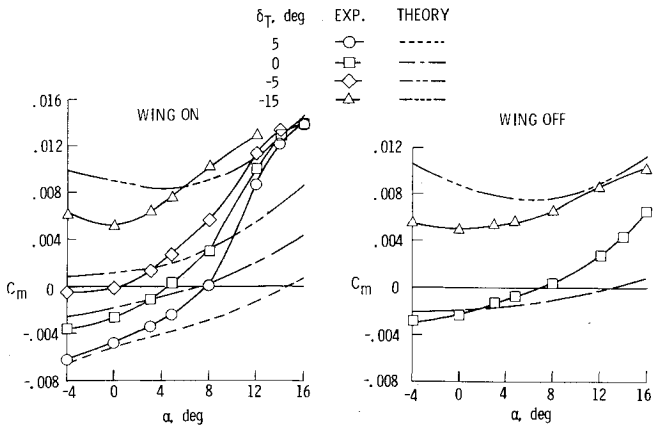

Fig. 5 Pitching moment characteristics of concept A without engine.

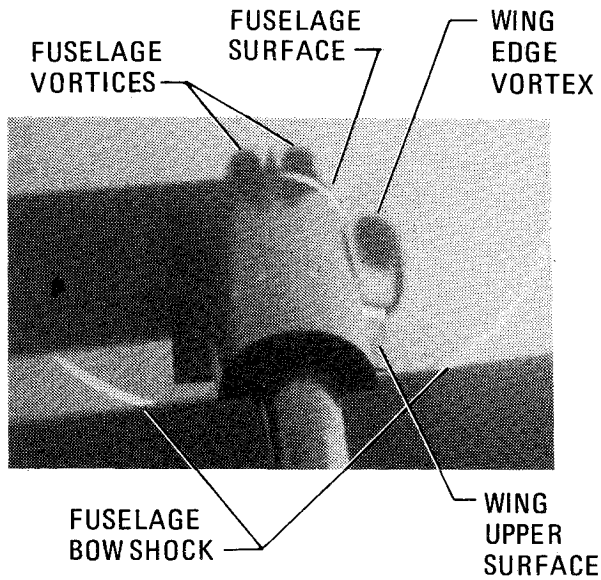

Fig. 6 Vapor screen photograph of concept A at $\alpha = 12$ deg.

body, and low, narrow wings similar to concept A. However, in order to accommodate a forward-looking radar, the nose of concept B has a fineness ratio 2.1 tangent ogive back to $x/l \approx 0.125$. The fuselage contours then began a transition to a flat bottom "D" shape at about $x/l = 0.313$. All-flying tails and stationary side fins were provided for stability and control. The semispan of the tails was approximately 69% greater than the wing.

The capture areas of the engines shown in Figs. 2 and 3 are considerably larger than that required for Mach 6 cruise conditions and were sized to provide good acceleration characteristics from Mach 4 staging. However, in bank-to-turn maneuvers where moderate to large angles of attack are required to obtain large normal load factors, the shock-layer thickness limits the inlet area for a given engine width. This situation becomes particularly critical for such "oversized" engines as the bow shock moves in toward the lower lip of the engine cowl. Since engine performance would be seriously degraded if the bow shock enters the cowl lip, the maximum angle of attack of such vehicles is limited to a large extent by the engine inlet height.

Stability, Performance, and Control

The aerodynamic performance characteristics of concept A are shown in Fig. 4. The lift and drag characteristics of this configuration without the engine were accurately predicted at low angles of attack; however, both parameters were overpredicted at the higher angles of attack partly because the tails and fins are shielded and situated in a low q environment. The

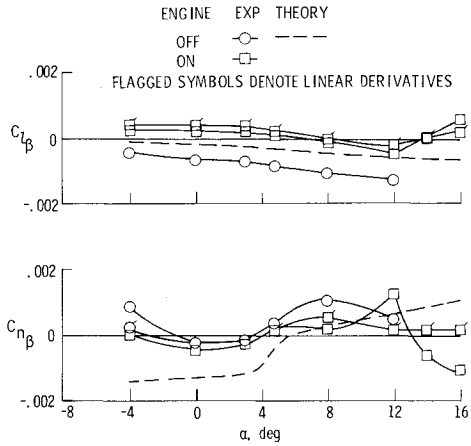

Fig. 7 Lateral and directional stability characteristics of concept A.

measured $(L/D)_{max}$ without engine was approximately 3.6 which is about 0.3 lower than the predicted value. Maximum lift-drag ratio was further reduced by approximately 0.8 with the two-module scramjet engine attached.

The pitching moment characteristics of concept A are shown in Fig. 5. This configuration had a negative $C_{m,0}$ ($C_L = 0$ at $\alpha = 3$ deg) and was unstable about a moment reference center located at 58% of the fuselage length. Rather severe pitchup was encountered which was not predicted theoretically. In addition, the tail-control power essentially vanished at the higher angles of attack. The right side of the figure shows the influence the wing has on pitching moment. With the wing removed, some of this high angle-of-attack control power is recovered and, in addition, there is a reduced pitchup tendency. These effects are partially due to the wing shielding the tails at high α (e.g., Ref. 5). However, vapor screen photographs of this configuration (e.g., Fig. 6) at the fuselage-tail, leading-edge juncture show a strong vortex formation at higher angles of attack. Since the horizontal tails were located in the vortex core, these vortices contribute to a loss in control effectiveness as well as the pronounced increasing C_{m_α} for $\alpha > 8$ deg with the wing on. Lee-side vortices have been observed previously on flat-bottom, delta-wing configurations with half-cone bodies at hypersonic speeds[6] and their existence on the narrow-wing, flat-bottom configuration of this study suggests the need for additional research on design parameters such as planform shape and placement of wings relative to the location of control surfaces. Although not investigated in this study, lee-side vorticity has been demonstrated to greatly increase local heating rates and thus present an additional factor to be considered in the thermal protection-system design.

The lateral-directional characteristics of concept A are shown in Fig. 7 with and without the flow-through engine. To emphasize the nonlinear character of the sideslip derivatives at high angles of attack, these derivatives were determined by 1) linear slopes between 0 and 4 deg β, and 2) actual slopes of the appropriate coefficient at $\beta = 0$ deg.

With engine off, the configuration was laterally stable over the test angle-of-attack range. The engine produced a nearly constant positive increment in C_{l_β} (i.e., adverse roll) up to $\alpha = 12$ deg at which point the increment begins to increase. The theoretical trend of C_{l_β} with angle of attack is correct for $\alpha \leq 12$ deg but the magnitude is only about half that measured.

The directional characteristics of concept A exhibit a more complex variation over the angle-of-attack range with regions of instability. Without the engine there appears to be a similarity between theory and experiment between $\alpha = 0$ deg and $\alpha = 8$ deg. Below $\alpha = 0$ deg the experimental data show an increase in C_{n_β} which is believed due to the fact that the fins are experiencing a higher than freestream dynamic pressure as

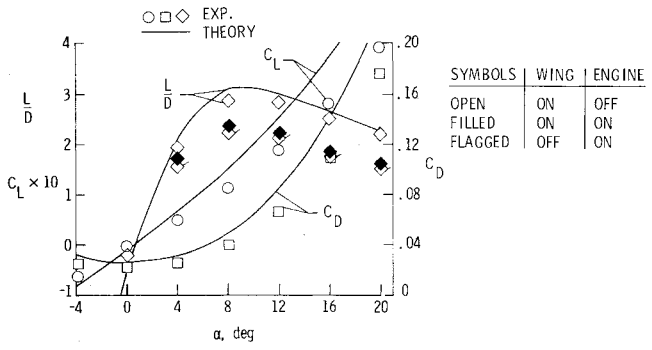

Fig. 8 Aerodynamic performance characteristics of concept B.

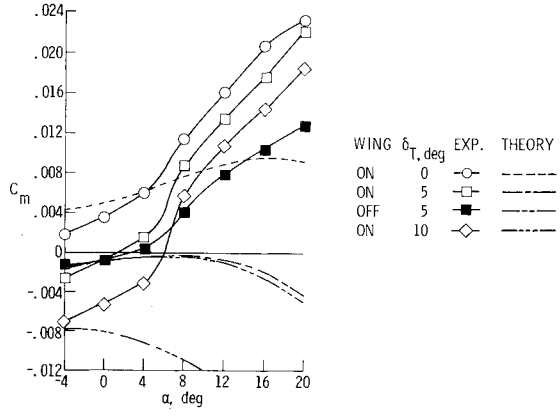

Fig. 9 Pitching moment characteristics of concept B without engine.

a result of the compressive flow on the upper part of the body. The divergence between theory and experiment above $\alpha = 8$ deg is attributed to the occurrence of the strong vortex on the wing upper surface.

The increased side area resulting from the addition of the engine did not cause a significant change in yawing moment below about 5 deg angle of attack. Beyond this angle of attack there were significant nonlinearities in the data such that the C_{n_β} indicated by the linear increment remained positive but the true slope changed sign between 12 and 14 deg.

These nonlinearities in yawing moment as well as the behavior of the rolling moment at the higher angles of attack may be associated with the wing vortex or pressure-field perturbations caused by the engine. Additional research and analysis will be required to identify and fully explain the behavior noted in these data. The predictions of C_{l_β} and C_{n_β} are, in general, consistent with those on other hypersonic vehicles (e.g., Ref. 7). The generally poor agreement is attributed to the inability of the theoretical approach to account for variations in local-dynamic pressure, shadowing of control surfaces at angle of attack, and component interference.

The aerodynamic performance characteristics of concept B are presented in Fig. 8. Both the lift-curve slope and drag characteristics of the configuration without the engine were overpredicted and the divergence increased with angle of attack. The maximum lift-drag ratio of 2.9 diminished by approximately 0.5 when the two-module scramjet engine and the flow fences were attached, and the removal of the wing only lowered the maximum lift-drag ratio by about 7%.

The pitching moment characteristics of concept B without the engine are presented in Fig. 9. With zero tail deflection, the vehicle had a positive $C_{m,0}$ ($C_L = 0$ at $\alpha = 0$ deg) and was unstable about a moment-reference center of 58% of the fuselage length. In addition, abrupt pitchup tendencies occurred above $\alpha = 4$ deg which the theory could not predict. Unlike concept A, concept B retained significant control

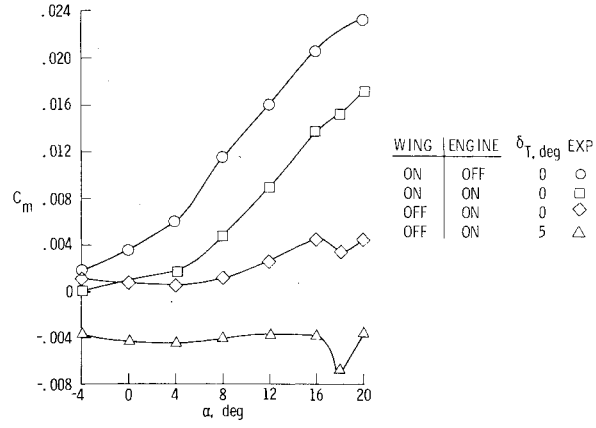

Fig. 10 Pitching moment characteristics of concept B, with and without wing and engine (engine includes exhaust-flow fence).

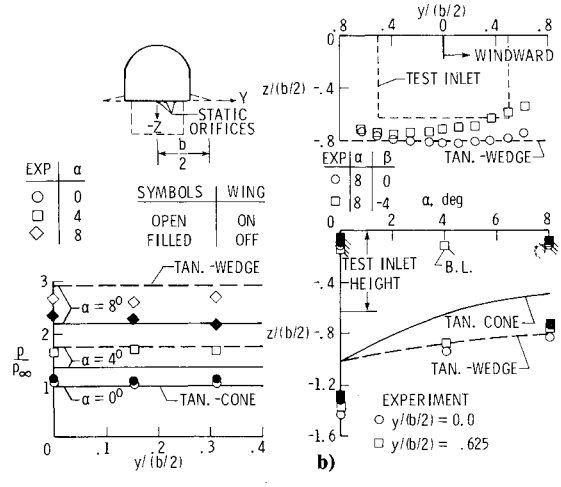

Fig. 11 Static pressures and shock shapes near inlet face of concept A. a) Static pressures; b) Shock shapes and boundary layer.

power at higher angles of attack. This difference is believed due to the more favorable longitudinal position of the horizontal tails on concept B relative to the wing trailing edge. Removal of the wing increased stability, and greatly diminished the pitchup tendency.

The pitching-moment characteristics of concept B with and without the wing and engine are presented in Fig. 10. The engine and flow fences slightly increased stability below $\alpha = 4$ deg and reduced C_m by a constant increment at higher angles of attack. Significant improvement in C_{m_α} was obtained by removing the wing and, with $\delta_T = 5$ deg, this configuration approaches neutral stability. The abrupt changes in pitching moment near $\alpha = 16$ deg are believed due to the ingestion of the bow shock by the engine as evidenced by Schlieren photographs.

The lateral-directional characteristics of concept B were similar to those that were discussed for concept A.

Surface Pressure and Flowfield Surveys

Spanwise pressure distributions on the flat lower surface of concept A are shown on the left of Fig. 11. The discrepancy between tangent wedge theory and experiment increases rapidly above 4 deg angle of attack due to pressure bleed-off toward the wing tip. Removal of the wing aggravates this situation even more and tangent-cone theory provides a better approximation for estimating the surface pressures without the wing.

The shock-layer height and boundary-layer thickness are shown as a function of angle of attack on the lower right of Fig. 11. With the wing on, it appears that the boundary-layer

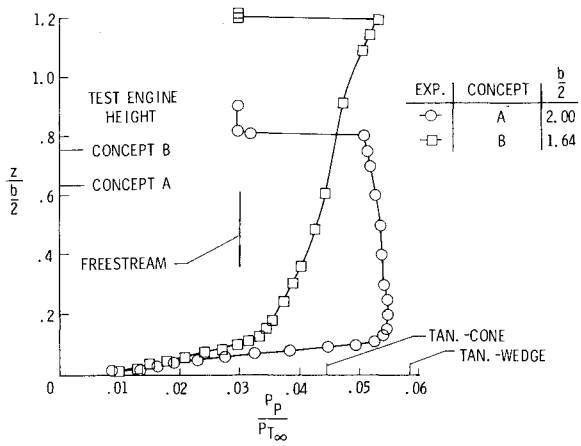

Fig. 12 Pitot profiles for concepts A and B, $\alpha = 8$ deg.

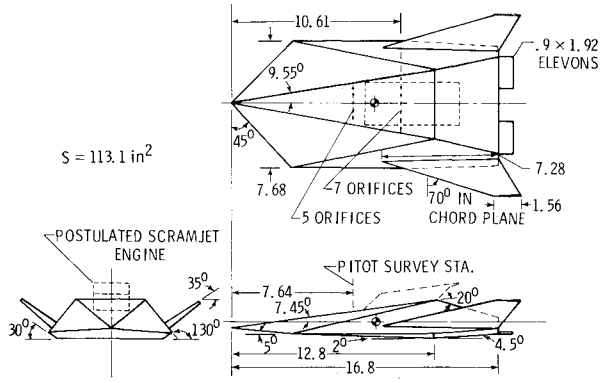

Fig. 13 Sketch of concept C, dimensions in inches.

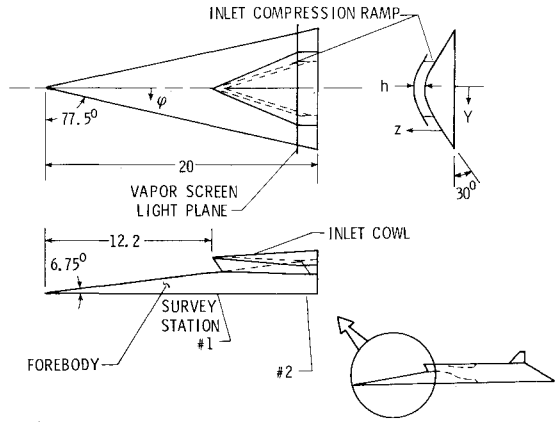

Fig. 14 Sketch of concept D, dimensions in inches.

thickness on the centerline is essentially unaffected by angle of attack; there does appear to be some decrease in thickness, however, when the wing is removed.

An accurate prediction of shock-layer thickness is important for bottom-mounted engines, especially in high normal force loading situations. As can be seen in Fig. 11, oblique-shock theory provides a good approximation for estimating this thickness above $\alpha = 4$ deg despite the fact that tangent-wedge theory overpredicts the surface-static pressures. The data at $y/(b/2)$ of 0.0 and 0.625 show that angle of attack had little effect on shock-layer curvature. Removal of the wing decreased the shock-layer thickness but even for this condition tangent-wedge theory provides a better prediction of shock-layer thickness than does tangent-cone theory.

As shown on the upper right of Fig. 11, sideslip had two effects on shock shape: first, it decreases the maximum shock-layer height and, secondly, it causes a significant reduction in the shock-layer height on the windward side of the configuration. The latter could be especially important for wide rectangular "oversized" inlets because of the possibility that the shock could impinge on the inlet causing flow nonuniformities and higher than anticipated local heating.

Figure 12 compares the experimental centerline pitot pressure survey results on the two bottom-mounted engine concepts at 8 deg angle of attack. The surveys were taken just upstream of the postulated inlet location and near the body midlength; however, based on wing semispan, the survey station for concept B is 22% rearward of the survey station for concept A.

The surveys results show that the ogival nose of concept B had a shock-layer height substantially greater than that of the flat-bottom configuration. Further, the greatest pitot pressure occurred at the bow shock with the ogival nose as opposed to near the body for the flat-bottom shape. These effects may be partially due to the more rearward position of the survey station in terms of wing semispan. From the point of view of preliminary engine sizing it is interesting to note that the flat-bottom concept achieved an average pitot pressure about halfway between a two-dimensional and conical compression. The average pitot pressure on the ogive-nosed vehicle, on the other hand, was much less than predicted by tangent-cone theory and indeed may be representative of more realistic configurations at hypersonic speeds. Further research is required to attain the best tradeoff between engine flowfield quality and overall vehicle characteristics.

Upper Surface Inlet or Engine Concepts

Concepts C and D

As shown previously in Fig. 1, two concepts with lee-side inlets were investigated. The first was a spatula-like configuration and a sketch of this concept (C) is shown in Fig. 13.

This shape was the result of a parametric study aimed at simultaneously achieving high aerodynamic performance ($L/D \approx 4.0$), good volumetric efficiency ($V^{2/3}/S \approx 0.23$) and stealth in a vehicle designed for long-range cruise at Mach 6. To accomplish these objectives the configuration had nearly a flat bottom with a modular engine situated on the upper surface to reduce observables. The vehicle was unusually wide to reduce the engine signature by shielding and to help preserve inlet flow two-dimensionality by reducing tip effects. The inlet of the conceptual engine was sized for essentially no forebody precompression, thus the cruise angle of attack was intended to be about 7.5 deg with respect to the vehicle reference axis. The upper-surface afterbody of this vehicle was envisioned as forming the external nozzle of a scramjet engine. Because the vector orientation of the exhaust nozzle force can have an important effect on pitching moment, definition of the afterbody angle must be determined by engine integration studies; nevertheless, for this configuration, it was chosen to be 20 deg with respect to the engine axis since this angle has been shown to be near optimum in previous engine integration studies (e.g., Ref. 8).

A 35 deg dihedral angle for the fins provided the largest theoretical increment in C_{l_β} with the smallest decrement in $(L/D)_{max}$. (A large dihedral effect was necessary to offset the adverse roll of the inward slope of the body flanks.) It was envisioned that these fins could be folded along the flanks of the fuselage, thus affording a very compact configuration for conveyance.

Pitch and roll control could be provided by trailing-edge controls on the fins or by body flaps; the latter method was investigated here. Due to a potential interference problem with the model support sting, the size of the body flaps was restricted to only about 3% of the planform reference area.

The second lee-side inlet concept (D) is shown in Fig. 14. This flat-iron shaped concept evolved from studies by McDonnell Douglas Astronautics East and was also designed

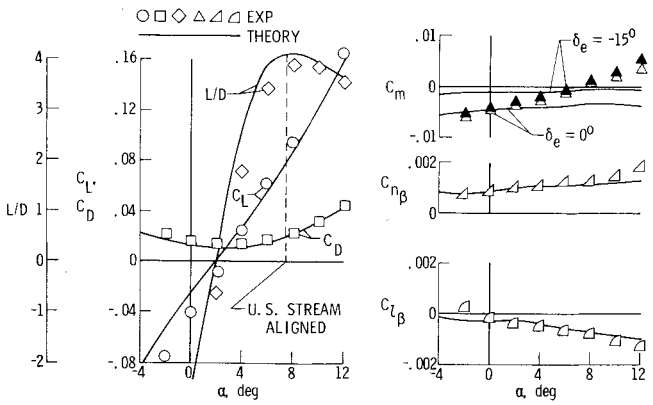

Fig. 15 Aerodynamic performance characteristics of concept C.

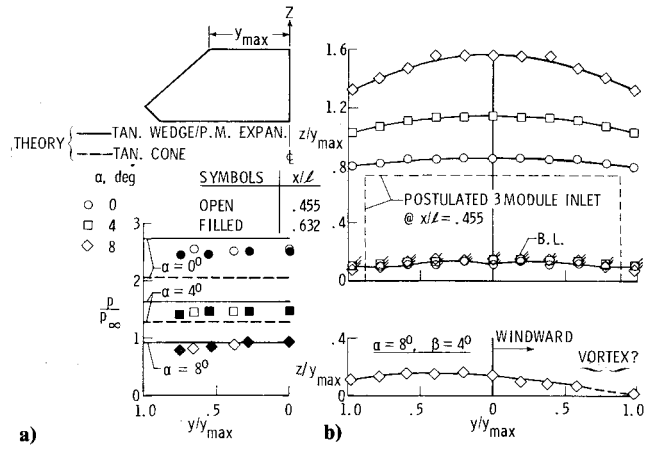

Fig. 16 Static pressures and shock shapes on upper surface of concept C. a) Static pressures; b) Shock shapes and boundary layer.

primarily from stealth considerations. It features a relatively large and highly integrated engine inlet which is intended to capture most of the lee-side flow, compress it in the lateral direction, and deliver it to two ramjet inlet throats situated outboard from the body centerline. The test model for this concept consisted of the forebody and the initial inlet ramps since only the inlet flow characteristics were investigated experimentally.

Stability, Performance, and Control

The aerodynamic performance characteristics of concept C are shown in Fig. 15. At the design angle of attack the vehicle achieved an L/D of 3.83 as compared to a predicted value of 4.08. With appropriate corrections to the upper surface-afterbody pressures due to the engine exhaust (a reduction in drag), flight-base pressure (an increase in drag) and the occurrence of limited regions of laminar flow in flight due to the low Reynolds number for the full-scale vehicle, it is possible that the initial objective of an L/D of 4.0 is achievable.

With a moment reference center at 54% of the fuselage length, the configuration was trimmed at the design angle of attack, but was 4.9% unstable. The magnitude of pitching moment at zero lift was predicted with reasonable accuracy; however, the theory indicated a more negative C_{m_α} than the data.

Elevon control power was extremely small and is believed to be due to the following factors: 1) the size restriction mentioned earlier, and 2) the choice of elevon location at the aft end of the body where only the lower surface is exposed to the flow. The theory employed here gave optimistic results for the control parameter C_{m_δ} because it used the isolated panel concept; a more realistic value could have been obtained by assigning a $C_p = -1/M_\infty^2$ to the elevon upper surface regardless of deflection angle. Clearly, a more effective method of control would have been partial or full span trailing-edge controls on the fins, in which case both the upper and lower surfaces would have been exposed to the stream.

Except for angles of attack below about -1 deg, the vehicle was stable both laterally and directionally. Moreover, the magnitude and trends of the sideslip derivatives were accurately predicted by the Hypersonic Arbitrary-Body Aerodynamics Program. This agreement is decidedly contrary to previous experience with the program and it is speculated that, unlike more slender distinct wing-body configurations which have wing and tail junctures immersed in thick fuselage boundary layers (especially where these components produce secondary shocks which interact with these boundary layers), the relatively large lateral dimensions of the spatula tend to subordinate these interactions and afford a more accurate definition of the sideslip derivatives C_{n_β} and C_{l_β}.

Surface Pressures and Flowfield Surveys

Because of concern about the quality of flow entering the lee-side engine, especially near the design angle of attack,

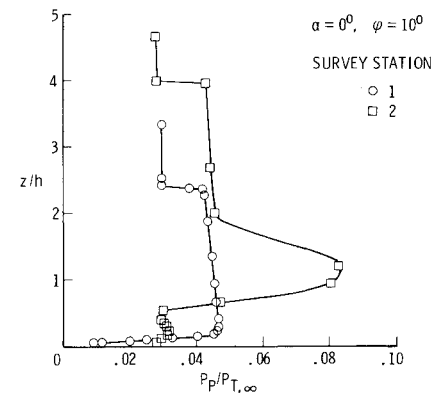

Fig. 17 Pitot profiles for concept D.

static-pressure distributions were measured over the forebody upper surface and pitot-pressure surveys were made just upstream of the postulated engine-inlet location. The pitot profiles for concept C were similar to those obtained on concept A and some of the data from these tests are shown in Fig. 16. The lateral static-pressure distributions are shown on the left as a function of the local forebody semiwidth at two fuselage stations. As can be seen at $\alpha = 8$ deg (about half a degree above the design angle of attack), the pressures near the body centerline were accurately predicted by Prandtl-Meyer theory. There was, however, a slight decay in pressure toward the edge of the forebody despite the fact that at this angle of attack the pressure on the flank of the body was, by impact concepts, designed to be higher than that on the forebody itself. The intent here was to eliminate boundary-layer cross flows as much as possible with the ensuing thinning of the boundary layer toward the forebody edge. As indicated by the pitot-pressure surveys at $\alpha = 8$ deg on the right of the figure, this effort was unsuccessful because the boundary-layer thickness at the most outboard station was only about half that near the body centerline.

The static-pressure distributions at angles of attack below 8 deg show less of a pressure decay toward the edge of the forebody with correspondingly less boundary-layer thinning; this is believed due to a more rapid increase in pressure on the body flanks as compared to the upper surface as the angle of attack diminishes.

Frequently, tangent-cone theory has been used on body windward surfaces in the Hypersonic Arbitrary-Body Aerodynamics Program because it (along with Prandtl-Meyer lee-side pressures) has given the best overall agreement with experimental data. As indicated in Fig. 16, however, the static pressure data lie between oblique shock and tangent-cone theories.

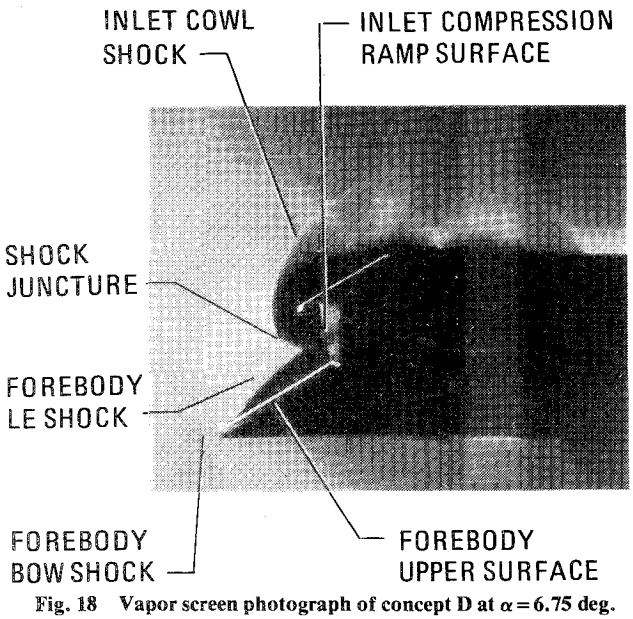

Fig. 18 Vapor screen photograph of concept D at $\alpha = 6.75$ deg.

Flowfield survey results on the right side of Fig. 16 indicate the forebody boundary-layer thickness to be about 19% of the postulated inlet height; the engine thrust would be reduced by the momentum defect appropriate to this thickness, which, for a 1/7 power profile, is about 3%.

Shock curvature at $\alpha = 8$ deg was considerably greater than at $\alpha = 0$ deg indicating more of a tendency toward three-dimensional flow at the higher angles of attack.

Boundary-layer survey results at $\alpha = 8$ deg in sideslip indicate the maximum height of the forebody-boundary layer shifted laterally by the tangent of the sideslip angle. The pitot profile near the windward forebody chine was unlike the remainder of the profiles leading to the suspicion that a vortex existed on the lee side of the chine.

Limited flowfield surveys were obtained on the forebody of concept D ahead of and adjacent to the simulated wedge-inlet ramps (Fig. 17). The pitot survey ahead of the inlet is smooth and shows some compression above the freestream level with the highest pressure occurring near the body; this type of distribution is quite similar to that measured normal to the surface of the flat bottom configuration (concept A: see e.g., Fig. 12).

The pitot-pressure survey in the presence of the inlet ramps indicates a dramatic change in the pressure distribution with evidence of large gradients over the height of the inlet. Oblique-shock theory indicates the upper surface leading-edge shock for this configuration will be detached at all angles of attack; thus it may be expected that the wedge inlet will be subjected to a very complex flow situation. The nature of the flow in the inlet is shown by the vapor screen photograph of Fig. 18. This figure suggests that the inlet-cowl shock intersects with a shock from the body leading edge to form a lambda shock at about the mid-height of the inlet. In addition, there is evidence of a rapid thickening of the boundary layer toward the body centerline so that almost half of the inlet height is submerged in this boundary layer. Thus, for Mach 6 conditions, additional tailoring is required to avoid the complex flow exhibited in Fig. 18.

Concluding Remarks

The stability, performance, and inlet flowfield characteristics of four hypersonic missile concepts have been investigated at Mach 6. Two of the concepts employed twin bottom-mounted engine modules and the remaining two were designed to incorporate top-mounted inlets and/or engines.

Vortices emanating from the slender, low wings and the effects of component shielding dominated the performance and especially the stability and control characteristics of the bottom-mounted engine concepts. Because impact theory does not account for either of these flowfield features, it could not accurately predict the aerodynamic characteristics of these configurations. The experimental results suggest the need for additional research on wing planform shape and placement as well as relative location of control surfaces.

The spatula-like concept designed to accommodate a lee-side engine provided good aerodynamic performance. Agreement between theory and experiment for this configuration was much better than for the bottom-mounted engine concepts because of weaker interactions between components. Control power was insufficient due to the limited size of the surfaces and their location at the fuselage trailing edge.

Inlet flowfield surveys indicated the flat-bottom configuration produced a nearly uniform pitot-pressure distribution normal to the body surface with a value about halfway between conical and two-dimensional theory. Conversely, the ogive-nosed vehicle had significant flowfield pressure gradients with average pressure over a representative engine height substantially below that predicted by cone theory. Because of its importance on engine sizing, the effect of nose shape on the flow uniformity and shock-layer height on hypersonic missile configurations warrants further research. The spatula-like concept exhibited uniform flow at the engine inlet while the upper surface-inlet concept with a highly-swept forebody incurred large gradients due to leading edge-inlet shock interactions.

References

[1] Hunt, J.L., Lawing, P.L., Marcum, D.C., and Cubbage, J.M., "Performance Potential and Research Needs of a Hypersonic, Airbreathing Lifting Missile Concept," *Journal of Aircraft,* Vol. 16, Oct. 1979, pp. 666-673.

[2] Krieger, R.J., "Aerodynamic Design Criteria for Supersonic Climb-Cruise Missiles," Paper 79-1671, Boulder, Colo., Aug. 1979.

[3] Billig, F.S., Waltrup, P.J., and Stockbridge, R.D., "The Integral-Rocket, Dual-Combustion Ramjet: A New Propulsion Concept," *Proceedings of the 4th International Symposium on Air Breathing Engines,* AIAA, N.Y. 1979, pp. 433-444.

[4] Gentry, A.E., "Hypersonic Arbitrary-Body Aerodynamic Computer Program (Mark III Version)," Rept. DAC 61552, Vols. I and II, April 1968.

[5] Anon, "Research-Airplane Committee Report on Conference on the Progress of The X-15 Project," NACA, Oct. 25-26, 1956, p. 39-56.

[6] Becker, J.V., "Studies of High Lift/Drag Ratio Hypersonic Configurations," *Proceedings of the Fourth Congress of the International Council of the Aeronautical Sciences,* Spartan Books, 1965, pp. 877-910.

[7] Penland, J.A., Dillon, J.L., and Pittman, J.L., "An Aerodynamic Analysis of Several Hypersonic Research Airplane Concepts from M = 0.2 to 6.0," *Journal of Aircraft,* Vol. 15, Nov. 1978, pp. 716-723.

[8] Weidner, J.P., Small, W.J., and Penland, J.A., "Scramjet Integration on Hypersonic Research Airplane Concepts," *Journal of Aircraft,* Vol. 14, May 1977, pp. 460-466.